Parameter analysis of atomized droplets sprayed evaporation in flue gas flow

Shuqin Feng[1], Liehui Xiao[1], Zhihua Ge[1†], Lijun Yang[1], Xiaoze Du[2,1†], Hongwei Wu[3]

1 Key Laboratory of Condition Monitoring and Control for Power Plant Equipment (North China Electric Power University), Ministry of Education, Beijing 102206, China

2 School of Energy and Power Engineering, Lanzhou University of Technology, Lanzhou 730050, China

3 School of Engineering and Technology, University of Hertfordshire, Hatfield, AL10 9AB, UK

Abstract

Spraying flue gas desulfurization (FGD) wastewater into the flue duct is a promising technology to achieve zero emission of wastewater by evaporation in thermal power plants. To deal with the scale and corrosion on flue gas duct walls resulted from the incomplete droplets evaporation, a substantiated combined Eulerian-Lagrangian model was developed to reveal the thermo-fluid behavior of the FGD wastewater in the flue gas. The influences of relating factors under various operating conditions were conducted by numerical simulations with experimental verifications. Considering numerous parameters have complex influences on the spraying evaporation of wastewater in flue gas duct, the LSSVM model based on the numerical data is employed for forecasting the droplet evaporation rat. **Seven dominate factors, including that of ???,** were analyzed to reveal their impacts on the droplets sprayed evaporation rate and distance, respectively. It is conclude that the spray direction of nozzles should be selected to enhance the relative movement between atomized droplets and flue gas, as well as good dispersion of the droplets, to

† Corresponding author. Tel.: +86(10)61773923; Fax: +86(10)61773877. Email address: gezh@ncepu.edu.cn (Z. Ge); duxz@ncepu.edu.cn (X. Du)

assure sufficient heat exchange with the flue gas in a specified distance and time and achieve the maximum evaporation. By considering all the influencing factors, the LSSVM prediction model on droplets evaporation has a high accuracy and can be carried out for the optimization of FGD wastewater droplets spray treatment technology under practical operating conditions in power plant.
Keywords: flue gas desulfurization wastewater treatment, spray evaporation, atomized droplets, Least-Square support vector machine (LSSVM) model

Nomenclature

A_d	Droplet surface area (m^2)
B_M	Mass Spalding number
B_T	Thermal Spalding number
C_D	Drag coefficient
c_p	Specific heat ($J\ kg^{-1}\ K^{-1}$)
D_m	Diffusion coefficient ($m^2\ s^{-1}$)
d_d	Droplet diameter (μm)
E	Internal energy ($J\ kg^{-1}$)
F	Forces acting on droplet (N)
F_D	Drag force (N)
g	Acceleration of gravity ($m\ s^{-2}$)
h_c	convective heat transfer coefficient ($W\ m^{-2}\ K^{-1}$)
$h_{i'}$	Sensible enthalpy of species i' ($J\ kg^{-1}$)
$J_{i'}$	Diffusing flux of species i' ($kg\ m^{-2}\ s^{-1}$)
k_f	Thermal conductivity of flue gas ($W\ m^{-1}\ K^{-1}$)
k_c	Mass transfer coefficient ($m\ s^{-1}$)
L_h	Latent heat of water vaporization ($J\ kg^{-1}$)
m_d	Droplet mass (kg)
Nu	Nusselt number
Pr	Prandtl number
P	Pressure (Pa)
Re	Reynolds number
S	Source term
S_e	Source term of energy ($W\ m^{-3}$)

S_m	Source term of mass (kg m^{-3} s^{-1})
S_{mo}	Source term of momentum (kg m^{-2} s^{-2})
Sc	Schmidt number
Sh	Sherwood number
T	Temperature (K)
u_f	Flue gas velocity (m s^{-1})
u_d	Droplet velocity (m s^{-1})
u_i u_j u_k	Flue gas velocity components (m s^{-1})
$Y_{i'}$	Mass fraction of species *i′*

Greek symbols

ρ	Density (kg m^{-3})
δ_{ij}	Mean strain tensor (s^{-1})
μ	Dynamic viscosity of flue gas (kg m^{-1} s^{-1})
Φ	Viscous dissipation (W m^{-3})

Subscripts

d	droplet
eff	effective
f	flue gas
i,j,k	Cartesian coordinate directions
i′	species
n	nozzle
t	time
s	surface

1. Introduction

Limestone-gypsum wet flue gas desulfurization (WFGD) process is commonly used in the flue gas desulfurization (FGD) systems of coal-fired power plants [1], which periodically discharges a certain amount of wastewater [2]. FGD wastewater is high contaminative and must be treated separately before discharging [3-6]. With the national increment of Hg as well as other heavy metal pollutants emissions and the gradually increasing environmental standards, zero discharge of FGD wastewater has attracted widely attention recently [1,7]. However, among the conventional FGD wastewater treatment methods, the traditional chemical precipitation method cannot effectively remove the high concentration of chloride contained in FGD wastewater. And the costs of advanced treatment process, such as biological treatment and steam concentration evaporation, are too high for sustainable operation. Besides, the evaporation pool needed in these processes is limited by regional climate and land area.

After chemical precipitation and concentration reduction, spraying FGD wastewater in flue duct and then evaporating by absorbing the residual heat of flue gas is an effective and economic treatment technology. Fig. 1 shows the process of spraying FGD wastewater in flue duct evaporation treatment technology. Firstly, compressed air is used to atomize FGD wastewater to be treated into droplets through nozzles. And then, the droplets are sprayed into the flue duct between the air preheater and precipitator and absorb the waste heat from flue gas to evaporate rapidly. After the complete droplets evaporation, the chemical content of atomized FGD wastewater droplets crystallizes as remaining suspended mini solid particles and are captured and removed by the follow-up dust collector, achieving the nearly zero emissions of FGD wastewater.

The wastewater sprayed evaporation technology has advantages such as sufficient heat exchange between droplets and flue gas, short time-consuming, energy saving and environmental friendly. However, it has been found that the non-fully evaporated atomized FGD wastewater droplets may contact with the flue duct walls or move to the downstream devices in some practical engineering

applications. The long-term operation with incomplete droplets evaporation can cause serious corrosion or severe fouling on flue duct, which may endanger the operation of boiler. Therefore, to obtain safe and effective long-term operation, it is imperative to determine the moving trajectory and evaporation characteristics of atomized FGD wastewater droplets injected into the flue duct. The key parameters include that of the time and distance required for complete droplets evaporation under different operating conditions.

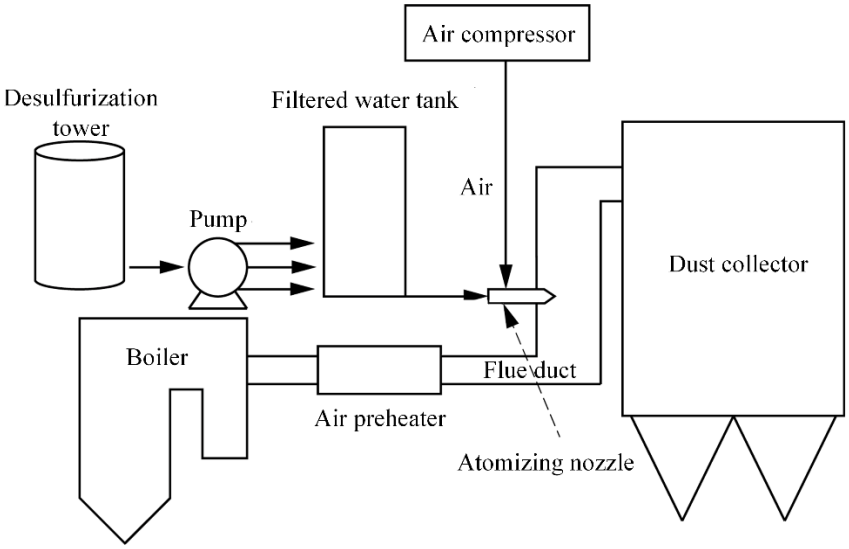

Fig. 1. The process of spraying FGD wastewater in flue duct evaporation treatment technology.

Over the past decades, many efforts have been made on droplets evaporation both numerically [8-13] and experimentally [14-17]. The influences of different parameters were investigated, including that of air velocity, air temperature and droplet size distribution. For example, Montazeri et al. [9] analyzed the impact of physical parameters on the performance of the water spray cooling system, and concluded that the cooling performance of the system is enhanced for wider drop-size distributions. Alkhedhair et al. [11-12] found that the spray dispersion is a major factor on the evaluation of a spray cooling system and described clear trends of cooling enhancement with low air velocity or small droplet size distribution. Kim et al. [18] studied the influence of ambient pressure on the evaporation of a spray, and reported that increasing the ambient pressure yields the

enhancement of a spray evaporation. Ashgriz et al. [19] proposed the regulars of convective motion between droplets and flue gas based on the atomized droplets evaporation characteristics, and found that low air velocity is benefit to the dispersion as well as the evaporation time of droplets.

However, literature review found that there were seldom researches on droplets evaporation aimed at improving the operation of spraying FGD wastewater evaporation in flue duct. Moreover, during the practical application, numerous parameters may influence the evaporation characteristics of atomized FGD wastewater droplets, such as the flow rate and spray direction of a spray nozzle. Since it is inconvenient and unrealistic to measure the droplet evaporation rate along the practical flue duct and take all the influencing factors into consideration simultaneously, it is difficult to optimize the spray evaporation.

The Least-Square Support Vector Machine (LSSVM) is a nonlinear, black-box regression method based on the structural risk-minimization principle [20]. By solving a set of linear equations instead of a convex quadratic programming problem for standard Support Vector Machines (SVMs), the LSSVM greatly simplifies the optimization processes under multi constraint conditions and reduces the computational burden. With the advantages of good robustness, high accuracy and excellent generalization, the LSSVM is suitable for small samples, nonlinearity, and high-dimensional data series forecasting in different applications [21-23]. However, it is seldom that the LSSVM model was used on forecasting the evaporation rate of droplets for spraying FGD wastewater in flue gas treatment process.

In the present study, a substantiated combined Eulerian-Lagrangian mathematical model is developed to calculate the thermo-fluid behavior of the FGD wastewater in the flue gas during evaporating process. The influence of the factors will be analyzed, such as the droplets size distribution, the flue gas velocity as well as the flow rate, full cone angle and spray direction of a spray nozzle. An optimized arrangement of spray nozzles is proposed to improve the droplets evaporation rate. Based on the achieved numerical results, a LSSVM model is introduced to

expeditiously predict the evaporation rate of droplets along the flue duct. The results can be used to guide the design of spraying FGD wastewater treatment technology.

2. Mathematical model and numerical approach

According to the application shown in Fig. 1, take the straight rectangular flue duct as the present physical model. The FGD wastewater to be treated is atomized into droplets by compressed air and sprayed into the flue gas flow through nozzles. The physical model is established based on a 300 MW coal-fired power generating unit. The domain for the computational investigation is based on the flue duct between the air preheater and dust collector. As shown in Fig. 2, for a single spray nozzle, the 3-D physical model is simplified as the channel size of 5 m long and 1×1 m^2 cross section. The coordinate of the model is established 0.5 m from the inlet at the center of the cross section. A single nozzle with a solid cone spray is simulated at the origin of coordinate and atomized droplets discharged from this nozzle travel in three dimensions in the model. The angle between nozzle spray direction and flue gas flow direction is defined as α.

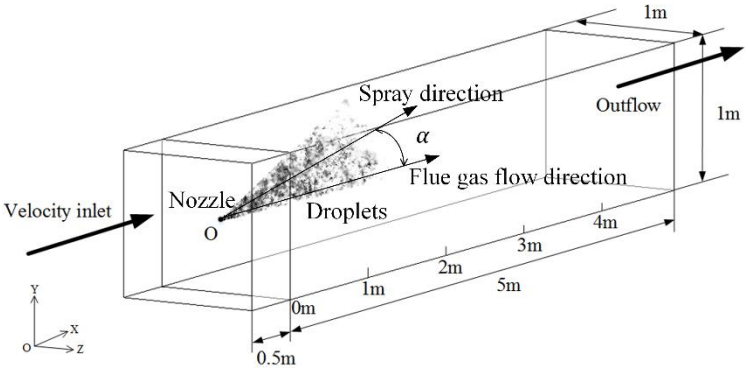

Fig. 2. Physical model.

2.1 Governing equations

For spray modelling purposes, the Eulerian-Lagrangian approach is used to describe the thermo-fluid behavior of atomized droplets in flue gas, by which the turbulent flow heat transfer of the continuous phase (flue gas) is described by the Eulerian framework and the evaporation of the

dispersed phase (water droplets) is described using the Lagrangian framework.

2.1.1 Continuous phase (flue gas)

The turbulent flow heat transfer of flue gas is described by the Eulerian approach. Some sensitivity analyses have been already performed to investigate the performance of turbulence models on the simulations results of water spray systems [24-25]. Li et al. [24] conducted a sensitivity study on CFD modeling of cocurrent spray-drying based on experiment, and the standard *k-ε* turbulence model was proved to be more accurate and suitable than other turbulence models on descripting gas flow turbulence in water spray systems. Montazeri et al. [25] studied a sensitivity analysis focused on the impact of the turbulence model for the continuous phase, and found that the realizable *k-ε* turbulence model was also considered suitable for modeling the continuous phase turbulence in a water spray system. Considering the reasonable accuracy of numerical results at low computational cost, the time-averaged Navier-Stokes conservation equations combined with the standard *k-ε* turbulent model are used to model the flue gas turbulence effects in this study. Due to the injection of a large number of atomized droplets into flue gas, it is required to consider the influence of evaporative droplets on the flue gas flow by introducing the mass, momentum and energy source terms of droplets into the respective governing equations of flue gas. The controlling equations of the flue gas phase are set up as follows,

$$\frac{\partial}{\partial x_i}(\rho u_i) = S_{\mathrm{m}} \tag{1}$$

$$\frac{\partial}{\partial x_j}(\rho u_i u_j) = \frac{\partial}{\partial x_j}[\mu_{eff}(\frac{\partial u_i}{\partial x_j} + \frac{\partial u_j}{\partial x_i}) - \frac{2}{3}\mu_{eff}\delta_{ij}(\frac{\partial u_k}{\partial x_k})] - \frac{\partial p}{\partial x_i} + \rho g_i + S_{\mathrm{mo}} \tag{2}$$

$$\frac{\partial}{\partial x_i}(\rho u_i E) = -p\frac{\partial u_i}{\partial x_i} + \frac{\partial}{\partial x_i}\left(k_{eff}\frac{\partial T_{\mathrm{f}}}{\partial x_i} + u_j(\tau_{ij})_{eff}\right) - \frac{\partial}{\partial x_i}\left(\sum_{i'=1}^{n} h_{i'} J_{i'}\right) + S_{\mathrm{e}} \tag{3}$$

$$\frac{\partial}{\partial x_i}(\rho u_i Y_{i'}) = -\frac{\partial J_{i',i}}{\partial x_i} + S_{\mathrm{m}} \tag{4}$$

where $J_{i',i}$ is the diffusion flux of species i', and the parameters S_{m}, S_{mo} and S_{e} represent the mass, momentum and energy sources terms of atomized droplets, respectively. Taking the influence of droplets on flue gas into account, these source terms are calculated by the Lagrangian framework in an alternate process through the volume averaging method and then incorporated into the Eulerian flue gas equations.

2.1.2 Discrete phase (water droplets)

Water sprayed from the nozzle will be disintegrated quickly into atomized droplets. A saturated flue gas-vapor layer will be formed on the surface of atomized droplets when droplets contact with unsaturated flue gas and the coinstantaneous heat and mass transfer will take place on the interface of the ambient flue gas and droplets. The heat and mass transfer between flue gas and droplets will occur due to the temperature difference existed between the droplet surface temperature and the flue gas dry-bulb temperature, while the vapor concentration gradient happened between the film of saturated air-vapor and the surrounding flue gas, respectively. It can be considered that the mechanism of heat and mass transfer in droplets evaporation is coincident with the single droplet evaporation mechanism with the assumption that the internal thermal resistance of droplets can be neglected. Thus, the rate of energy absorbed by each droplet can be described as,

$$m_{\mathrm{d}} c_{\mathrm{p}} \frac{\mathrm{d}T_{\mathrm{d}}}{\mathrm{d}t} = h_{\mathrm{c}} A_{\mathrm{d}} (T_{\mathrm{f}} - T_{\mathrm{d}}) - \frac{\mathrm{d}m_{\mathrm{d}}}{\mathrm{d}t} L_{\mathrm{h}} \tag{5}$$

where m_{d} is the droplet mass, c_{p} is the specific heat of droplet, T_{d} is the droplet temperature, A_{d} is the droplet surface area, L_{h} is the water latent heat for vaporization and T_{f} is the flue gas temperature. h_{c} is the convective heat transfer coefficient between flue gas and atomized droplets.

Based on the sensitivity study on CFD modeling of cocurrent spray-drying, the Ranz-Marshell empirical equation was proved to be more accurate on modeling water droplet evaporation [24].

Considering that the evaporation of droplets has great influence on the results, a corresponding Nusselt number *Nu* is used to describe droplets heating in the presence of evaporation. The Nusselt number is expected to be proportional to $Re_{\mathrm{d}}^{0.5}Pr^{0.33}$ [26] and the most widely used value of the coefficient is 0.6 [27]. Thus, h_{c} can be obtained by the Ranz-Marshell empirical equation for *Nu* [28],

$$Nu = \frac{h_{\mathrm{c}} d_{\mathrm{d}}}{k_{\mathrm{f}}} = \frac{\ln(1+B_{\mathrm{T}})}{B_{\mathrm{T}}}(2+0.6Re_{\mathrm{d}}^{0.5}Pr^{0.33}) \tag{6}$$

where *Nu* and *Pr* are the Nusselt number and Prandtl number of flue gas, respectively. k_{f} is the thermal conductivity of flue gas, d_{d} is the instantaneous average diameter of droplet, and Re_{d} is the droplet Reynolds number based on the relative velocity of droplet with respect to flue gas and the droplet diameter. B_{T} is the thermal Spalding number while B_{M} is the mass Spalding number, both of which can be written as,

$$B_{\mathrm{T}} = B_{\mathrm{M}} = \frac{Y_{\mathrm{i',s}} - Y_{\mathrm{i',f}}}{1 - Y_{\mathrm{i',s}}} \tag{7}$$

where $Y_{\mathrm{i',s}}$ is the vapor mass fraction of component *i'* on the surface of droplet while $Y_{\mathrm{i',f}}$ is the vapor mass fraction of component *i'* in the surrounding flue gas. $\mathrm{d}m_{\mathrm{d}}/\mathrm{d}t$ is the mass flow rate of droplet transferred to flue gas by evaporation, which indicates the droplet evaporation rate and can be expressed as [28],

$$\frac{\mathrm{d}m_{\mathrm{d}}}{\mathrm{d}t} = k_{\mathrm{c}} A_{\mathrm{d}} \rho_{\mathrm{f}} \ln(1+B_{\mathrm{M}}) \tag{8}$$

where ρ_{f} is the density of flue gas. k_{c} is the mass transfer coefficient, which can be obtained by the empirical Sherwood correlation [29-30],

$$Sh = \frac{k_{\mathrm{c}} d_{\mathrm{d}}}{D_{\mathrm{m}}} = 2 + 0.6Re_{\mathrm{d}}^{0.5}Sc^{0.33} \tag{9}$$

where *Sh* is the mass transfer Sherwood number, *Sc* is the Schmidt number, and D_{m} is the vapor

diffusion coefficient.

The trajectory and evaporation of atomized droplets are described utilizing the Lagrangian method by integrating the motion equations complied with Newton's second law and including the impact of the relevant forces from the flue gas. The forces acting on droplets from flue gas are so many including drag force, gravity, buoyancy, Magnus force, Saffman force and pressure gradient forces such as Basset effect and thermophoresis, etc. Based on the assumptions that all droplets are of independent properties and in a uniform spherical shape, changes in the velocity and direction of droplets in flue gas are mainly caused only by drag and gravity in the simulations, ignoring the effects of other forces on flow conditions. Thus, the instantaneous motion equation of a single droplet can be expressed as [31-32],

$$\frac{\mathrm{d}\vec{u}_\mathrm{d}}{\mathrm{d}t} = F_\mathrm{D}(\vec{u}_\mathrm{f} - \vec{u}_\mathrm{d}) + \frac{\vec{g}(\rho_\mathrm{d} - \rho_\mathrm{f})}{\rho_\mathrm{d}} \tag{10}$$

where $\vec{g}$ is the acceleration of gravity, $F_\mathrm{D}(\vec{u}_\mathrm{f} - \vec{u}_\mathrm{d})$ is the drag force per unit droplet mass, which can be written in terms of the drag coefficient as [33],

$$F_\mathrm{D} = \frac{18\mu}{\rho_\mathrm{d} d_\mathrm{d}^2}\frac{C_\mathrm{D} Re_\mathrm{d}}{24} \tag{11}$$

where C_D is the drag coefficient. According to the different range of Reynolds number, C_D can be expressed as [34],

$$C_\mathrm{D} = \begin{cases} 0.424 & Re > 1000 \\ \dfrac{24}{Re}\left(1 + \dfrac{1}{6}Re^{0.67}\right) & Re \le 1000 \end{cases} \tag{12}$$

The Rosin-Rammler model is used to model the size distribution of droplets [9, 35]. This model assumes an exponential relationship between the droplet diameter d_d and the mass fraction of droplets with diameters greater than d_d, which can be written as,

$$Y_\mathrm{d} = e^{-\left(d_\mathrm{d}/\bar{d}_\mathrm{d}\right)^n} \tag{13}$$

where Y_d is the mass fraction of droplets with diameters greater than d_d. n is the spread parameter as an indicator of the distribution width, which can be derived from Eq. (13) for each diameter group by averaging over the values. $\bar{d}_d$ is the mean diameter, the value of which equals d_d when $Y_d=e^{-1}$.

Y_d can be obtained from the mass density distribution $f_M(d_d)$, which can be expressed as [36],

$$f_M(d_d) = \frac{N_0 m}{M_0} f_N(d_d) \tag{14}$$

where $f_N(d_d)$ is the number density distribution related to $f_M(d_d)$, m is the mass of a single droplet of diameter d_d and density, N_0 and M_0 are the total number and total mass of the sample droplets, respectively.

In this study, the smallest and largest droplet diameter to be considered in the size distribution of the Rosin-Rammler model are 20 μm and 100 μm, respectively. Four groups of the mass density distribution are acquired based on an experiment with Phase Doppler Anemometer (PDA) system by the manufacturer of the nozzle. Thus, four groups of the Rosin-Rammler distribution of droplet size can be obtained through Eq. (13) and Eq. (14). The Parameters of Rosin-Rammler model used to describe the size distribution of droplets are presented in Table 1.

Table 1. The Parameters of Rosin-Rammler model used to describe the size distribution of droplets.

Parameters	Distribution 1	Distribution 2	Distribution 3	Distribution 4
the mean diameter (μm)	24.79	45.08	64.05	84.84
the spread parameter	1.27708	2.38151	3.23307	3.55871

The O'Rourke's method is used to consider the droplet collisions of the spray calculation by a stochastic estimate [37-38]. This algorithm makes the assumption that two parcels may collide only if they are located in the same continuous-phase cell. The method of O'Rourke is second-order accurate at estimating the chance of collisions. The probability distribution of the number of

collisions follows a Poisson distribution, which is given by

$$P(n) = e^{-\bar{n}} \frac{\bar{n}^n}{n!} \tag{15}$$

where n is the number of collisions between a collector and other droplets.

2.2 Boundary conditions and operating parameters

Under the condition of engineering requirements, the model contains the assumptions that the influence of both the solid particles contained in FDG wastewater atomized droplets and the fly ash in flue gas on droplets evaporation are all neglected. But the collisions and clusters between wastewater droplets are taken into consideration. The boundary conditions and operating parameters of the continuous phase and discrete phase are described respectively.

2.2.1 Continuous phase (flue gas)

In this paper, the flue gas between the air preheater and the dust collector of a 300MW boiler tail flue duct is studied. The temperature and velocity of flue gas are T_f=393.15 K ~ 403.15 K and u_f=9 m/s ~ 10 m/s, respectively. Considering the practical operating conditions and parameters of thermal power plant boilers, the extended flue gas temperature and velocity are set at T_f=393.15 K ~ 453.15 K and u_f=6 m/s ~ 15 m/s, respectively. The specific thermal physical properties of flue gas at different temperatures are presented in Table 2 [39].

Table 2. Thermal physical properties of flue gas at standard atmospheric pressure [39].

Physical parameters	Temperature	Density	specific heat	thermal conductivity
Unit	T, K	ρ, kg·m^{-3}	c_p, J·kg^{-1}·K^{-1}	λ, W·m^{-1}·K^{-1}
flue gas	393.15	0.9096	1073.8	3.306×10^{-2}
flue gas	413.15	0.8692	1079.6	3.482×10^{-2}

flue gas	433.15	0.8288	1085.4	3.658×10^{-2}
flue gas	453.15	0.7884	1091.2	3.834×10^{-2}

The continuous phase is regarded as an ideal flue gas mixture containing water vapor, oxygen and nitrogen. The mass fractions of the components are $\omega_{CO2} = 0.13$, $\omega_{H2O} = 0.11$ and $\omega_{N2} = 0.76$, respectively. The inlet boundary condition for flue gas is set as velocity inlet condition, ensuring the inlet flue gas flow has a uniform and steady velocity. The temperature and velocity values of inlet flue gas calculated in the simulations are set independently under different conditions. While the outlet boundary condition is specified as fully developed outflow condition and the exit flow pressure is assigned at atmospheric pressure. The gravitational acceleration is set at -9.81 m/s^2 in the positive direction of *y*-axis. All the computational domain side walls are prescribed as adiabatic walls with no-slip velocity boundary condition.

2.2.2 Discrete phase (water droplets)

Based upon the operating parameters from a 300 MW power plant, the temperature, density and total solids content of FGD wastewater are 323.15 K, 1074 kg/m^3 and about 0.80%, respectively.

Droplets are injected by an individual spray nozzle (Type ST-1/8) with radius 0.02 m in a solid cone. This type of nozzle is suitable for viscous liquid and can finely adjust the flow rate, droplet size, spray distribution and coverage by adjusting the independent gas and liquid atomization lines. Moreover, the flow rate, spray full cone angle and spray direction of nozzle in the simulations are set independently under different conditions. The droplets are tracked in terms of parcels of droplets. In order to accurately characterize the droplets evaporation, a total of 300 specified parcels representing atomized droplets are set to describe the spray adequately and accurately, each of which contains a number of particles with the same characteristics in size, shape, speed, temperature, etc. And the turbulent dispersion of atomized droplets is taken into account by

implementing a stochastic trajectory tracking method with 5 tries for each parcel. The droplets are assigned with a uniform temperature 323.15 K while the initial average diameter and velocity of droplets in the numerical computations are set independently under different conditions. The distribution of droplets size obeys the Rosin-Rammler distribution. Moreover, based on a sensitivity analysis, 20 diameters are assumed to be sprayed from each droplet stream into the computational domain. The inlet and exit boundary condition for droplets are both set as “escape” while the wall boundary condition is defined as “trap”, which means that the simulation of droplets will be terminated and excluded from further calculation once the droplets hitting the walls.

Additionally, the evaporation process of atomized droplets is simplified as follows. Droplets have spherical shape and remain spherical during the entire evaporation process. Once collisions and clusters are taken place between wastewater droplets, it is assumed that a new spherical droplet forms according to the total volume. The vaporization latent heat, specific heat capacity and other parameter values of droplets are all change with droplets temperature, respectively. The impact of radiation heat transfer between flue gas and droplets on droplets evaporation can be ignored.

2.3 Numerical approach and validation

2.3.1 Numerical method

A staggered grid solution method is used with the SIMPLE algorithm for the pressure and velocity coupling. The spatial discretization scheme utilized is the second order upwind for more reliable and robust results in simulation.

The flue gas is modelled as a steady, incompressible and turbulent flow and water droplets as steady flow. The whole simulation is divided into two steps. Firstly, the flue gas flow field is calculated before adding the injection source. After obtaining a stable flue gas flow field, atomized droplets are then sprayed into the flue gas for further calculation. In the simulation, the interphase coupling method is used to calculate the influence of heat and mass transfer on flue gas due to the

evaporation of atomized droplets and vice versa. Through the interaction between flue gas and droplets, the force, trajectory and particle size distribution of droplets in flue gas flow field are calculated to further determine the key technical parameters that affect the movement and evaporation of droplets. The maximum iteration step is set at 50000 steps to obtain converged results in simulation. The continuous-phase flue gas flow field is calculated 10 steps per iteration while the atomized droplets are added into the flue gas and performs one step iteration calculation. The gas-liquid two-phase flow are alternately calculated until the monitoring parameters reach the convergence criterion.

2.3.2 Grid dependency validation

GAMBIT software is used to mesh the physical model and the computational grid is a mesh made from hexahedral elements. The grid refinement is constructed near the nozzle (the spray area) and along the channel (the atomized droplets diffusion area) to allow more accurately simulating where the exchange of momentum, mass and heat between flue gas and droplets is the largest. Several sized grids are carried out to examine the model grid dependency. A grid independence test is studied to investigate the cell edge lengths in the range 0.005-0.1 m in the direction of *x*-axis. Fig. 3 shows the effect of the number of cells on the evaporation rate of droplets at *x*=3 m cross section.

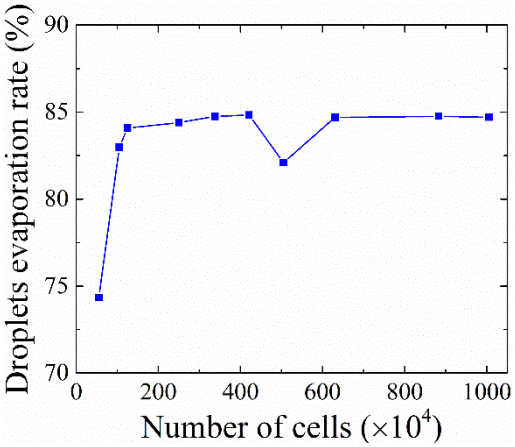

Fig. 3. Effect of the number of cells on droplets evaporation.

The data from Fig. 3 manifests that the evaporation rate of droplets rises up at the beginning with the increase of grid numbers and remains stable afterwards within a certain range of grid numbers. In unsteady simulations, the detailed calculating results will be influenced by mesh encryption, while the overall trend of iteration results will not change significantly. Since the evaporation rate of droplets at x=3 m cross section is selected as the grid validation index in the present study, there is a case where the detailed result is fluctuate. However, although the evaporation rate of droplets changes by about 4% with the number of cells from about 4 million to about 5 million, this fluctuation value is within the allowable error range for the complex two-phase flow in a spray system in engineering applications. In addition, with a further increase in the number of cells over about 5 million, the trend of the simulation results is consistent with that of fewer number of cells. It can also be seen from the figures that the evaporation rate of droplets is similar when the number of cells is within 1 250 000 to 4 210 000. Moreover, the maximum relative error of droplets evaporation rate in this range of cells number does not exceed 0.41%.

To achieve a good balance between simulation accuracy and computational effort, the model is meshed with the grid size of 0.01 m in the direction of both y-axis and z-axis, while the cell edge length in the direction of x-axis is 0.1 m in inlet domain and about 0.02 m in refined regions, respectively. Consequently, there will be a total of 2 500 000 cells in the model. Fig. 4 presents the global and local resulting grid structure of the computational model.

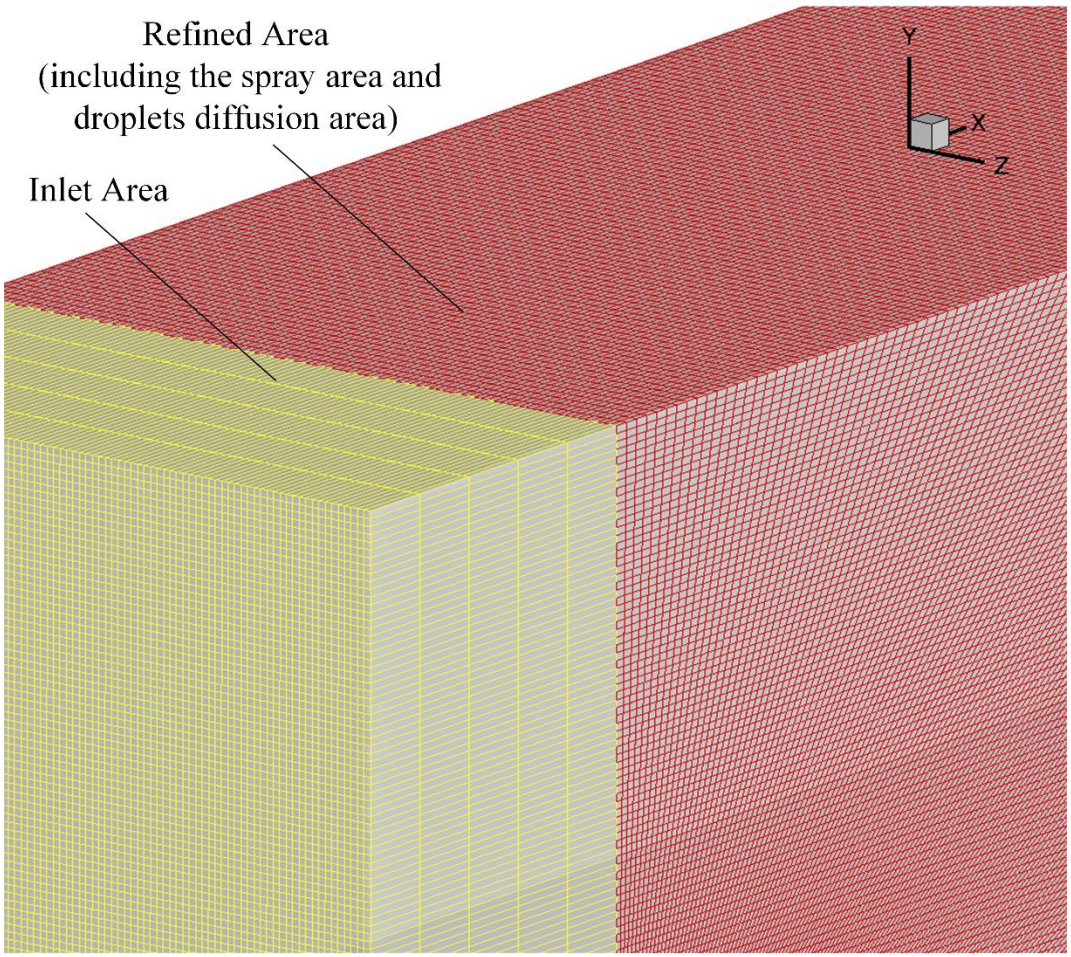

Fig. 4. Grid structure of the computational model.

2.3.3 Experimental validation using single droplet evaporation

An experiment on the evaporation of a single water droplet suspended in dry air was conducted by Ranz and Marshall in 1952 [30]. Evaporation rates and heat transfer of the single water droplet were obtained by a micro-technique in which the droplet with 110 μm diameter was suspended upward-flowing stream of air. The droplet with decreasing diameters was evaporated in hot air streams and the rate of evaporation was observed through a microscope and recorded on motion picture film. Based on the assumption that the internal thermal resistance of droplets can be neglected, it can be considered that the mechanism of heat and mass transfer in droplets evaporation is coincident with the single droplet evaporation mechanism. Therefore, in order to validate the confirmation of mathematical model and numerical approach, the spray of a single droplet with 110

μm diameter is simulated under the numerical conditions set to be consistent with the experimental conditions. The numerical results are compared with the experimental data in Ref. [27] as shown in Fig. 5. It can be seen that both the numerical and experimental data show the same result that the diameter of the single droplet gradually decreases with the increase of time. Moreover, the trend of simulation results is in keeping with the experimental results, and the maximum relative error between the numerical and experimental data does not exceed 10%, validating that the calculation model can accurately and credibly capture the evaporation rate of the single droplet.

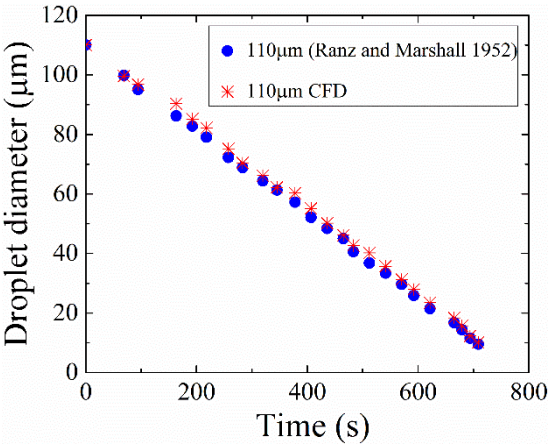

Fig. 5. Comparison of the single droplet diameter between experimental data and simulation results.

3. Least-Square Support Vector Machine prediction model

The basic prediction principle that is based on the LSSVM regression can be described as follows. Take the data from the numerical cases as the training data and test data, respectively. Consider a given set of *N* training samples $\{x_i, y_i\}_{i=1}^{N}$, where $x_i \in R^n$ is an n-dimensional input training sample and $y_i \in R^n$ is the output for training samples. And the training data needs to be linearly normalized to value between 0 and 1 before training the prediction model as follows,

$$x_i' = \frac{x_i - x_{\min}}{x_{\max} - x_{\min}} \tag{16}$$

where $x_{\max}$ and $x_{\min}$ are the maximum and minimum training data, respectively. x_i' is the processed

data.

The Gauss radial basis function (RBF) is selected as the kernel function in this paper and can be denoted by,

$$K\left(x_i, x_j\right) = \exp\left(-\frac{\left\|x_i - x_j\right\|^2}{2\sigma^2}\right) \tag{17}$$

where σ represents the width of the RBF kernel function.

The objective optimization function of the LSSVM algorithm can be expressed as [20],

$$\min_{\omega,b,e} J\left(\omega, \mathrm{b}, e\right) = \frac{1}{2}\omega^T\omega + \gamma\frac{1}{2}\sum_{i=1}^{N} e_i^2 \tag{18}$$

$$s.t. \quad y_i = F\left(x_i\right) = \omega^T\varphi\left(x_i\right) + b + e_i, \quad i = 1, 2, \mathrm{L}\ , N \tag{19}$$

where γ is the regularization coefficient for controlling the fitting error of the regression function, e_i is the prediction error, $\varphi(\cdot): R^n \to R^{nh}$ is a nonlinear function of mapping the input data to a high-dimensional space, and $\omega \in R^{nh}$ is the weight vector. The prediction error and the bias value satisfy $e_i \in R$ and $b \in R$, respectively.

The LSSVM model can be obtained at a new point x_i by,

$$y\left(x\right) = \sum_{i=1}^{N} \alpha_i K\left(x, x_i\right) + b \tag{20}$$

where α_i is the corresponding sample (x_i, y_i), which is called a support vector and is nonzero in all support vector coefficients.

The average relative error (ARE) and the root mean square error (RMSE) are regarded as the test criteria for performance measures of the prediction models. The ARE and RMSE can be calculated respectively by,

$$ARE = \frac{1}{N}\sum_{i=1}^{N}\left|\frac{y_i - \hat{y}_i}{y_i}\right| \times 100\% \tag{21}$$

$$RMSE=\sqrt{\frac{\sum_{i=1}^{N}\left(y_i-\hat{y}_i\right)^2}{N}}\times 100\% \tag{22}$$

where y_i denotes the actual droplet evaporation rate, $\hat{y}_i$ is the predicted droplet evaporation rate, and N is the total number of data points.

4. Results with analysis

The properties of atomized wastewater droplets, flue gas and nozzle are the main parameters affecting the droplets evaporation. By using controlling single variable method, this study conducts numerical simulation researches on influencing factors of droplet evaporation rate, including that of the diameter and velocity of droplets, the velocity of flue gas as well as the spray flow rate, spray full cone angle and spray direction of nozzle. The droplet evaporation rate at various distances along the computed domain is investigated respectively under different inlet flue gas temperatures. The parameters values of the reference cases studied are presented in Table 3. It should be noted that the droplets diameter obeys the Rosin-Rammler distribution, of which the average diameter of each distribution was displayed in Table 3.

Table 3. The parameters values of the reference cases**.**

Parameters	Case 1	Case 2	Case 3	Case 4	Case 5	Case 6
Droplets diameter (μm)	24.79, 45.08, 64.05, 84.84	64.05	64.05	64.05	64.05	64.05
Droplets velocity (m/s)	15	10, 20, 30, 40, 50, 60	15	15	15	15
Flue gas velocity (m/s)	9	9	6, 9, 12, 15	9	9	9
flow rate of a spray	30	30	30	10, 20, 30,	30	30

nozzle (L/h)				40, 50, 60		
full cone angle of a spray nozzle	30°	30°	30°	30°	30°, 40°, 50°, 60°, 70°, 80°, 90°	30°
Nozzle spray direction	0°	0°	0°	0°	0°	0°, 30°, 45°, 60°, 90°

4.1 Outline descriptions of wastewater droplets evaporation in flue duct

Fig. 6 shows the temperature fields of flue gas at different cross sections in the computational domain. The temperature and velocity of inlet flue gas are T_f=393.15 K and u_f = 9 m/s, respectively. The initial temperature, diameter and velocity of atomized droplets sprayed parallel to the flow direction of flue gas are T_d=323.15 K, d_d=64.05 μm and u_d = 15 m/s, respectively. The full cone angle and flow rate of a spray nozzle are β=30 ° and L_n=30 L/h, respectively.

It can be seen that the temperature in the center is the lowest and gradually increases to both sides. This is mainly because that the concentration of droplets sprayed conically from the nozzle is much higher and the droplets evaporation is faster and greater in the middle of the channel than that of other regions, causing that the temperature of flue gas in the middle region drops more greatly. What's more, it also can be found that the minimum temperature of flue gas at the central area in the computational domain exit section is 385.33 K and the descent range of temperature does not exceed 10 °C in the whole domain, of which the temperature is higher than that of the acid dew point of the flue gas. Obviously, it can prevent the scale and corrosion on duct walls and subsequent equipment of boiler tail duct.

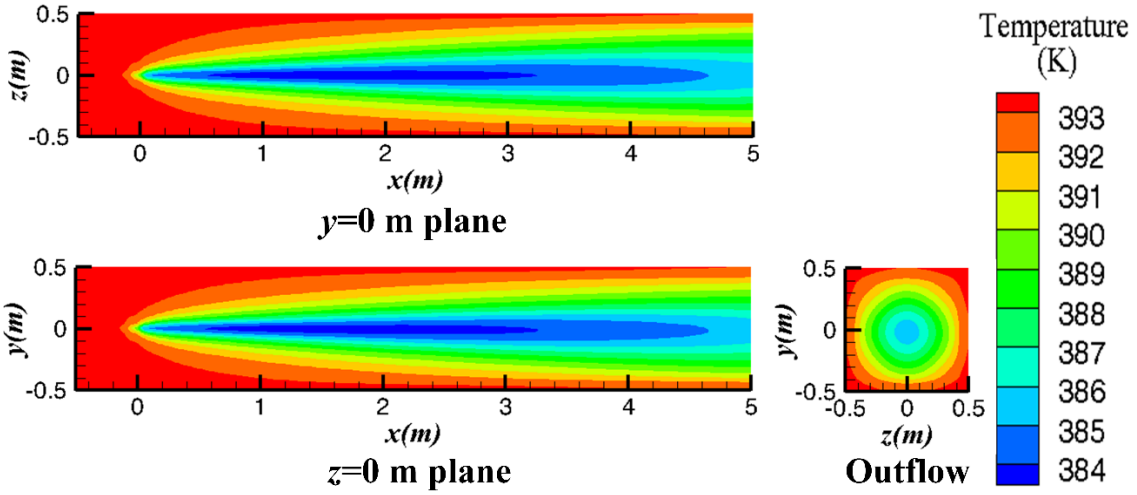

Fig. 6. The temperature field of flue gas during wastewater droplets evaporation.

The flow field of the evaporated droplets in flue duct is shown in Fig. 7. It can be seen that the droplet velocity is the fastest when they are ejected from the nozzle, and then the droplet velocity decreases rapidly to that of the flue gas along the duct. This is because the inertia of atomized droplets with tiny size is relatively small. In the flue gas flow, the droplet velocity will quickly decay to the flue gas velocity and then droplets are entrained by flue gas until they completely evaporate. It can also be seen that the trajectory of atomized droplets is biased slightly in the negative *y*-axis direction along the flue duct, owing to the effect of gravity.

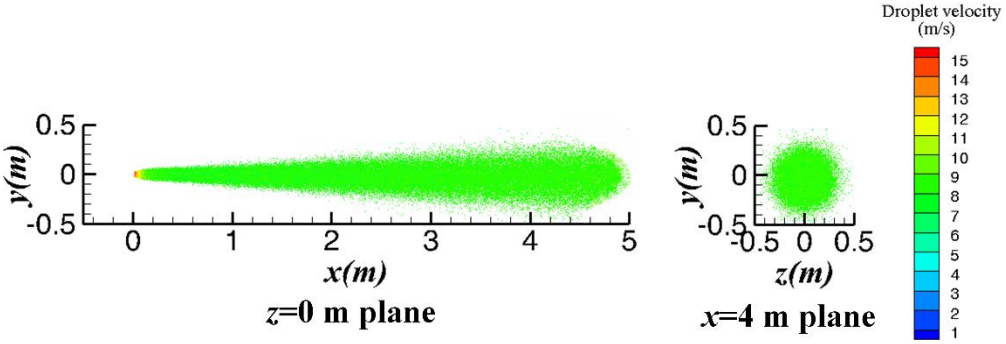

Fig. 7. The flow field of evaporated droplets along the flue duct.

Fig. 8 indicates the concentration distribution of atomized droplets at different evaporation distances in the *x*-axis direction under this condition. It can be seen that the atomized droplets

diffuse gradually and evaporate rapidly with increasing distance, leading to the gradually decreased droplets concentration.

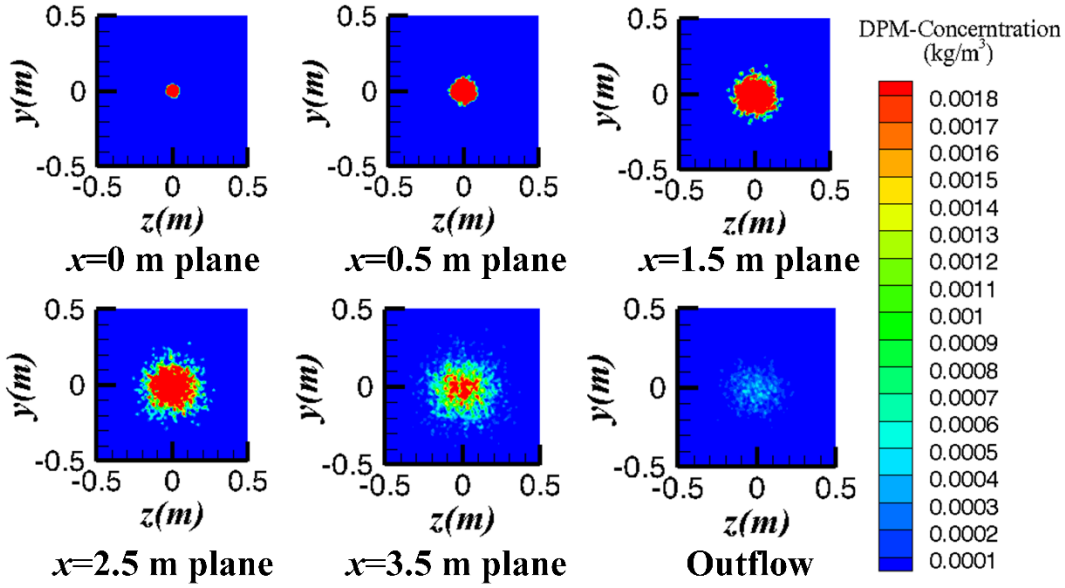

Fig. 8. The concentration fields of droplets at different cross sections.

Fig. 9 shows the Sauter mean diameter distribution of atomized droplets along the flue duct. Considering the influence of droplet collisions, it can be seen that the Sauter mean diameter of droplets decreases at first and then increases and then finally decreases. The result of droplet collisions depends on the Weber number of the droplet. Droplets with higher velocity have larger Weber number and smaller surface tension, resulting in break up after droplet collisions. Due to the high Weber number, droplets mainly break up after collisions at the initial atomization, resulting in a drop in the Sauter mean diameter of the droplets. And due to the small inertia, droplets with small diameter will reach to the flue gas velocity and be entrained by the flue gas rapidly. Thus droplets with smaller Weber number mainly coalesce after collisions, leading an increase in the Sauter mean diameter of the droplets. Droplets absorb the heat of the flue gas during the progress of evaporation, making the Sauter mean diameter of the droplets decrease eventually.

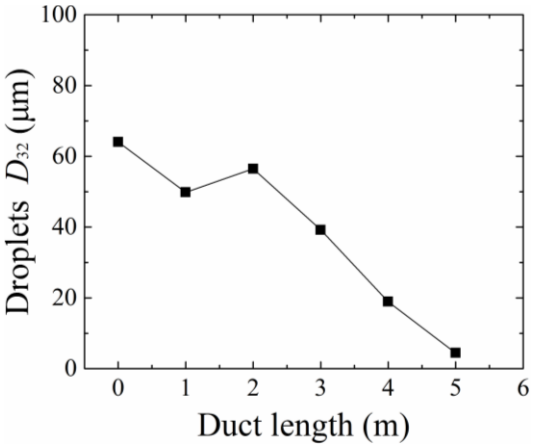

Fig. 9. The Sauter mean diameter distribution of atomized droplets.

4.2 Effects of influencing factors

4.2.1 Initial diameter of atomized droplets

The initial average diameter of atomized droplets is a key parameter of spray characteristic and affects the droplets evaporation significantly. The reference case has already been introduced in Table 3 as Case 1. The droplets evaporation at various distances along the computed domain obtained for various droplet sizes under different inlet flue gas temperature conditions are shown in Fig. 10.

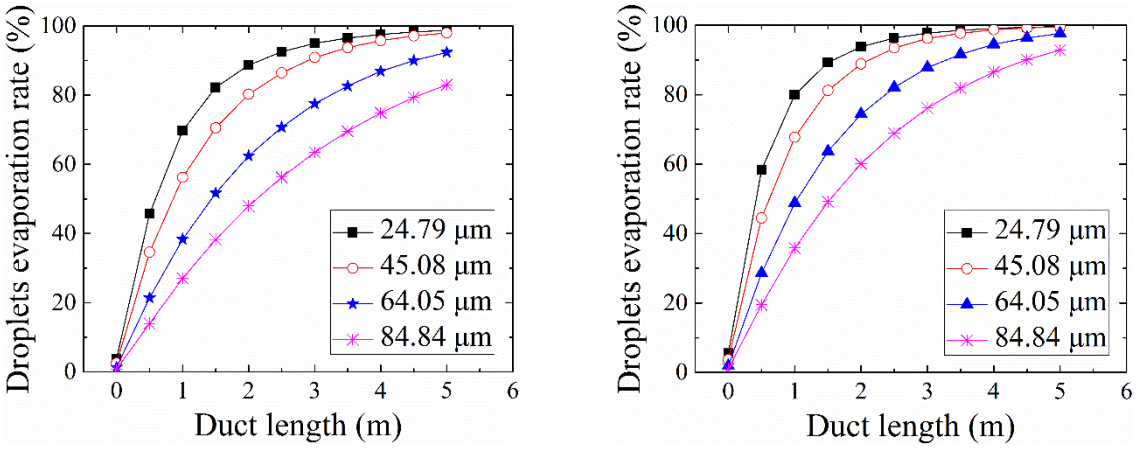

(a) T_f=393.15 K (b) T_f=413.15 K

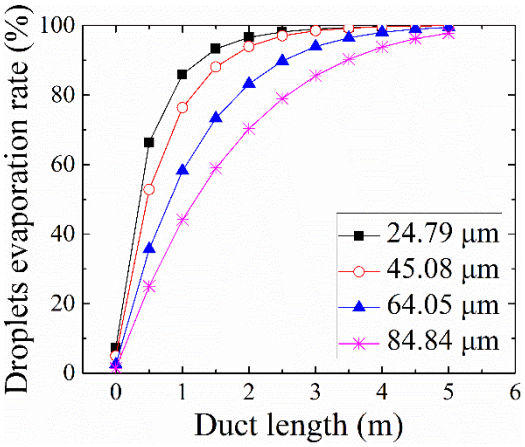

(c) T_f=433.15 K

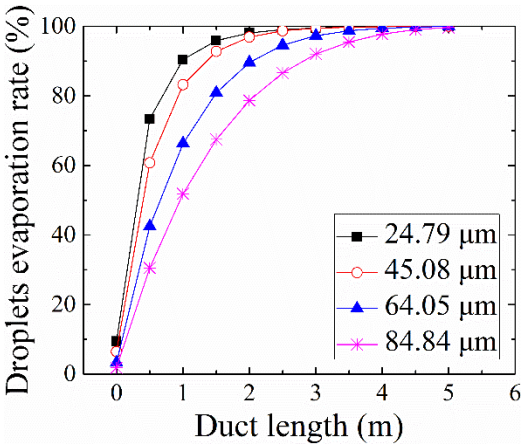

(d) T_f=453.15 K

Fig. 10. The evaporation rate of atomized droplets with different diameter.

It is evident that the distance required to achieve complete evaporation of atomized droplets with identical diameter is reduced as the inlet flue gas temperature increases. Moreover, atomized droplets with smaller diameter need shorter distance for complete vaporization at the same inlet flue gas temperature, contributing to higher evaporation rate. For instance, atomized droplets of 24.79 μm to 64.05 μm in diameter can all evaporate completely within the flow length of 5 m with inlet flue gas temperature 393.15 K as shown in Fig. 10. The main reason of these phenomena is that atomized droplets with smaller diameter have larger specific surface area, which can contribute to stronger convective heat transfer between flue gas and droplets when the gas-liquid two-phase flow moves relatively. Due to the intense heat transfer, it is more favorable for atomized droplets to absorb the heat from flue gas to evaporate rapidly.

4.2.2 Velocity of atomized droplets

The reference case has already been introduced in Table 3 as Case 2. The effect of droplet velocity is investigated by comparing six droplet velocities under different inlet flue gas temperature conditions.

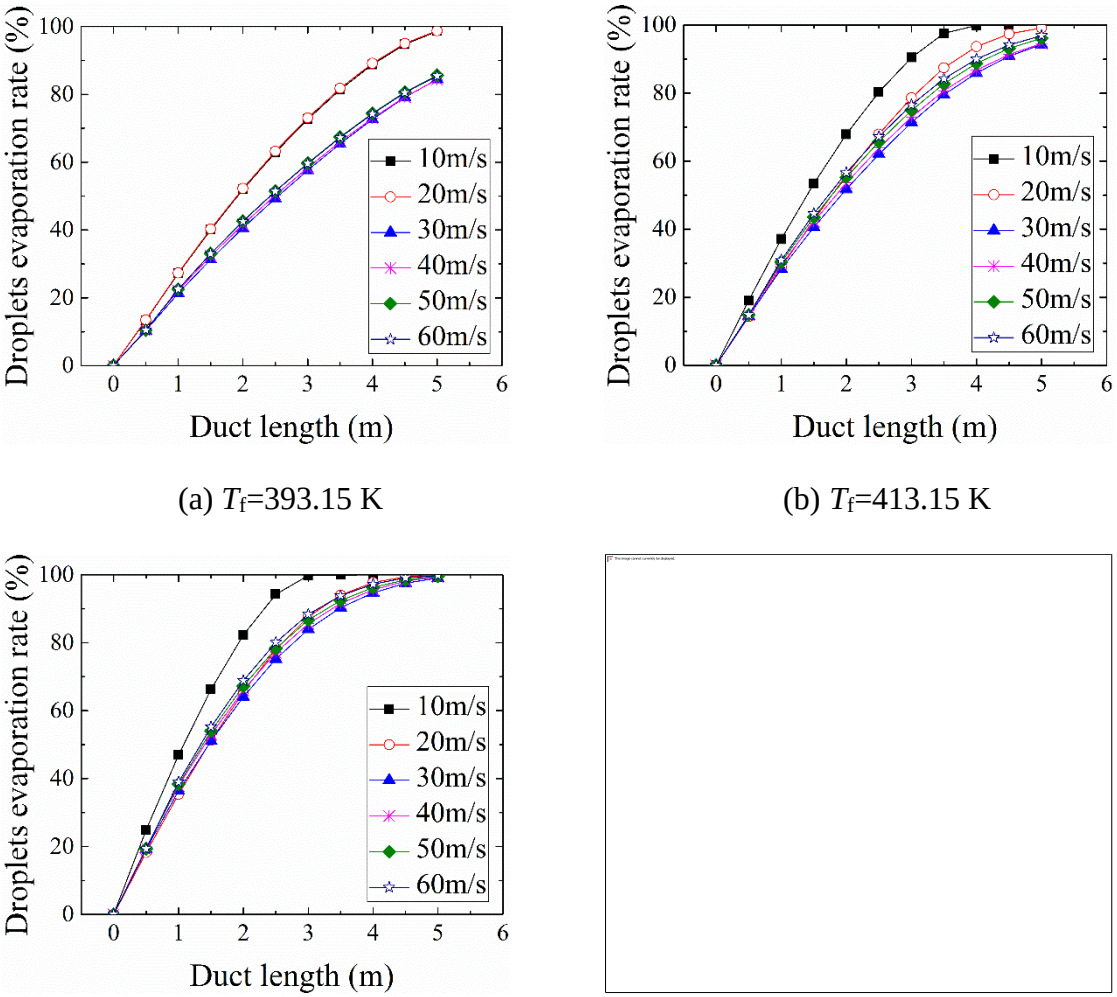

(a) T_f=393.15 K (b) T_f=413.15 K

(c) T_f=433.15 K (d) T_f=453.15 K

Fig. 11. The evaporation rate of atomized droplets with different initial injection velocities.

The same regularity of droplets evaporative rate with different inlet flue gas temperature is illustrated in Fig. 11. In the velocity range from 10 m/s to 30 m/s, the evaporation rate of atomized droplets decreases significantly with the increase of droplet spray velocity. This is primarily because that the droplet residence time in flue gas is shortened within this spray speed range, reducing the total quantity of heat exchange between flue gas and droplets and resulting in a drop in the droplet evaporation rate.

However, it can also be seen from Fig. 11 that the droplets evaporation is improved when the initial spray velocity of atomized droplets is further increased within the spray speed range from

more than 30 m/s to 60 m/s. This is due to the fact that the diffusion of atomized droplets is the major factor affecting droplets evaporation within this range of jetting velocities. Theoretically, the droplet residence time in flue gas is relatively short when the initial spray velocity of atomized droplets is high enough. Nevertheless, since the initial droplet velocity is high enough to make the spraying conical surface sufficiently large, the atomized droplets with a good dispersion ability resulting in a more effective mixing can fully contact and exchange heat with flue gas within a specified distance and time, which is beneficial to the improvement of droplets evaporation.

In summary, different initial droplet spray velocities will have a certain impact on droplets evaporation but the effect can be ignore. The excessive low injection speed will reduce the droplet evaporation rate to a certain extent. Thus, selecting the appropriate type of nozzle to increase the initial spray velocity of atomized droplets can ensure the dispersion of droplets, achieving better droplets evaporation.

4.2.3 Velocity of flue gas

The reference case has already been introduced in Table 3 as Case 3. The effect of the velocity of flue gas is studied comparing four flue gas velocities under different inlet flue gas temperature conditions. The droplet evaporation rates are shown in Fig. 12.

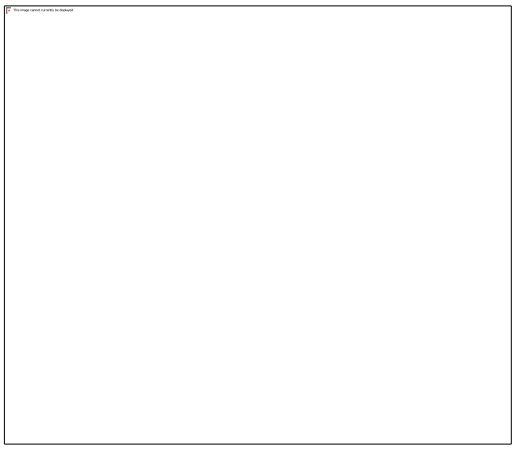

(a) T_f=393.15 K

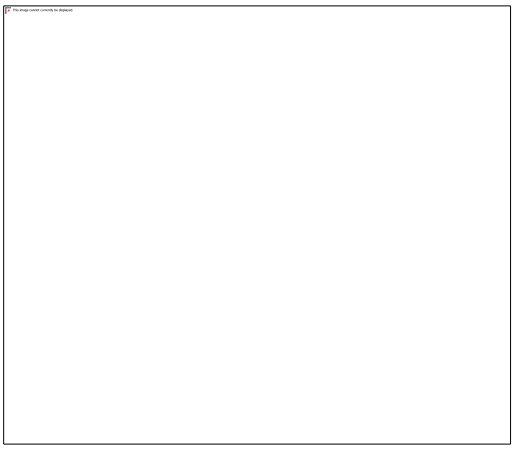

(b) T_f=413.15 K

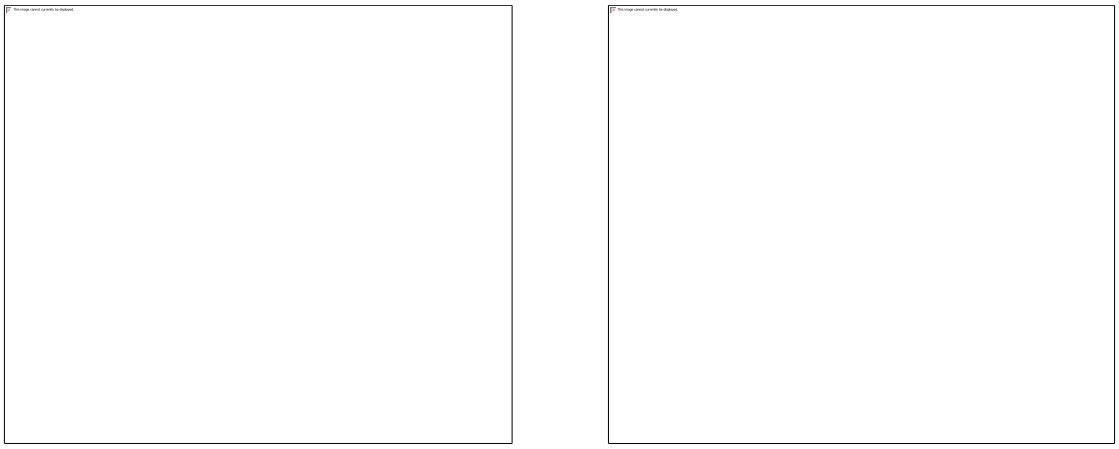

(c) T_f=433.15 K (d) T_f=453.15 K

Fig. 12. The evaporation rate of atomized droplets at different flue gas velocities.

It can be seen from Fig. 12 that the maximum droplets evaporation can be achieved at a flue gas velocity of 9 m/s. This is due to the fact that the relative motion and the convection heat transfer intensity between flue gas and droplets are the major factor affecting droplets evaporation under this value of flue gas velocity. When the flue gas velocity is in the range from 6 m/s to 9 m/s, the increase of flue gas velocity not only has an influence on the trajectory of atomized droplets but also strengthens the relative motion and the convection heat transfer intensity between flue gas and droplets, improving the droplets evaporation. In addition, the flue gas flow rate will rise up with the appropriate increase of flue gas velocity when the flow area of duct is constant. Thus, the flue gas with lower humidity comes into contact with the droplets, which can also contribute to enhance the relative movement between flue gas and droplets and improve the droplets evaporation. Hence, improving the flue gas velocity within a certain range can be beneficial to shorten the complete evaporation time and achieve better droplets evaporation.

However, it can also be seen from Fig. 12 that when the value of flue gas velocity exceeds 9 m/s, the droplet evaporation rate will decrease significantly with the flue gas velocity increased excessively. This is primarily because that the droplet residence time in flue gas is the key influencing factors on droplet evaporation rate under this range of the flue gas velocity. Due to the

high flue gas velocity, atomized droplets with small diameter and inertia will reach to the flue gas velocity and be entrained by flue gas rapidly. Thus, the value of droplets evaporation constant will be decreased and the convection heat transfer of two-phase flow will be weakened, which will reduce the total quantity of heat exchange between flue gas and droplets. Therefore, the droplet residence time in flue gas is shortened, deteriorating the evaporation of droplets resulting in a drop in the droplet evaporation rate.

In summary, different flue gas velocities will have a certain impact on droplets evaporation. The excessive flue gas velocity will reduce the droplet evaporation rate to a certain extent. Thus, spraying the flue gas desulfurization wastewater at a position where the flue gas velocity is low in the duct is advantageous for the complete evaporation of droplets and the implementation of this technology.

4.2.4 Flow rate from spray nozzle

The reference case has already been introduced in Table 3 as Case 4. The droplet evaporation rates under different inlet flue gas temperature conditions are shown in Fig. 13 by setting different nozzle spray flow rates.

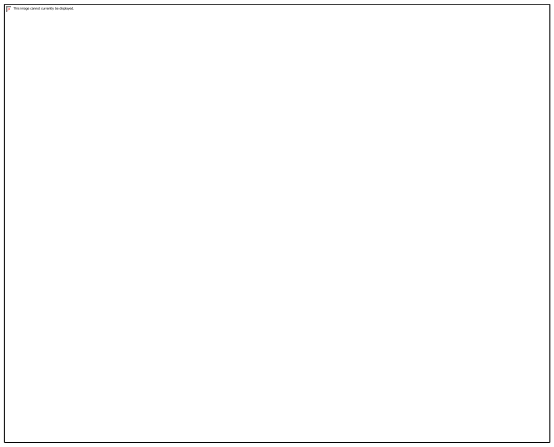

(a) T_f=393.15 K

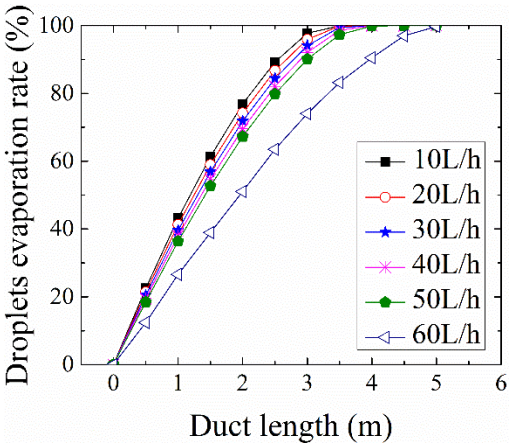

(b) T_f=413.15 K

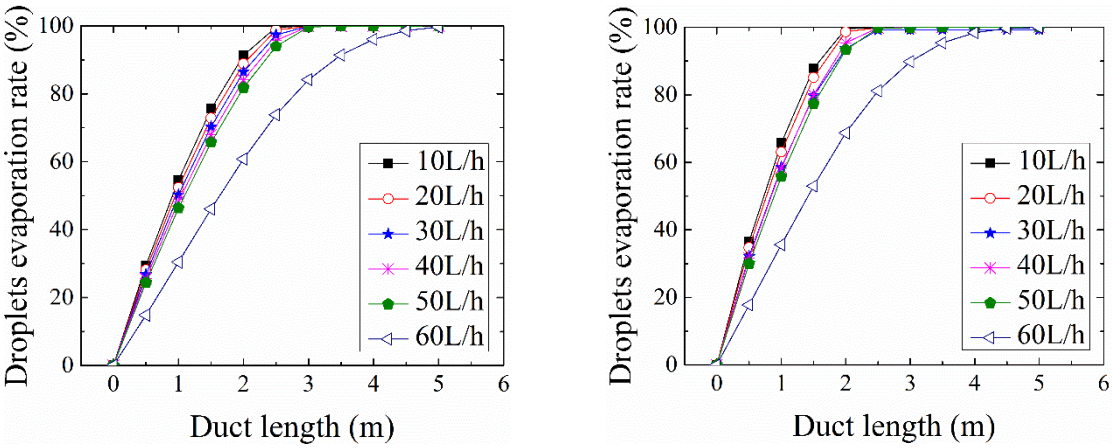

(c) T_f=433.15 K (d) T_f=453.15 K

Fig. 13. The evaporation rate of atomized droplets at different nozzle spray flow rates.

In the present study, the nebulized droplets do not encounter any of the computational domain side walls within the range of nozzle spray flow rate. As shown in Fig. 13, it is obvious that the droplet evaporation rate decreases and the droplets evaporation deteriorates as the nozzle jet flow rate increases. This is mainly because that the number of droplets to be evaporated will increase with the increasing nozzle spray flow rate, leading to poor droplet diffusion. Thus, the atomized droplets cannot fully contact and exchange heat with flue gas during the droplets movement along with the flue gas. Moreover, due to the insufficient heat provided by flue gas, it also shows the phenomenon of incomplete droplets evaporation within a 5 m evaporation distance under large nozzle spray flow rate conditions, which means that the distance needed to achieve complete droplets evaporation with large nozzle jet flow rate should be increased. The results put emphasis that an improved arrangement of multiple nozzles having small flow rate can be proposed to achieve better droplets evaporation if the cross-section of flue duct is large enough.

4.2.5 Spray full cone angle of nozzle

The reference case has already been introduced in Table 3 as Case 5. Fig. 14 illustrates the droplet evaporation rates affected by different nozzle spray full cone angle under different inlet flue

gas temperature conditions.

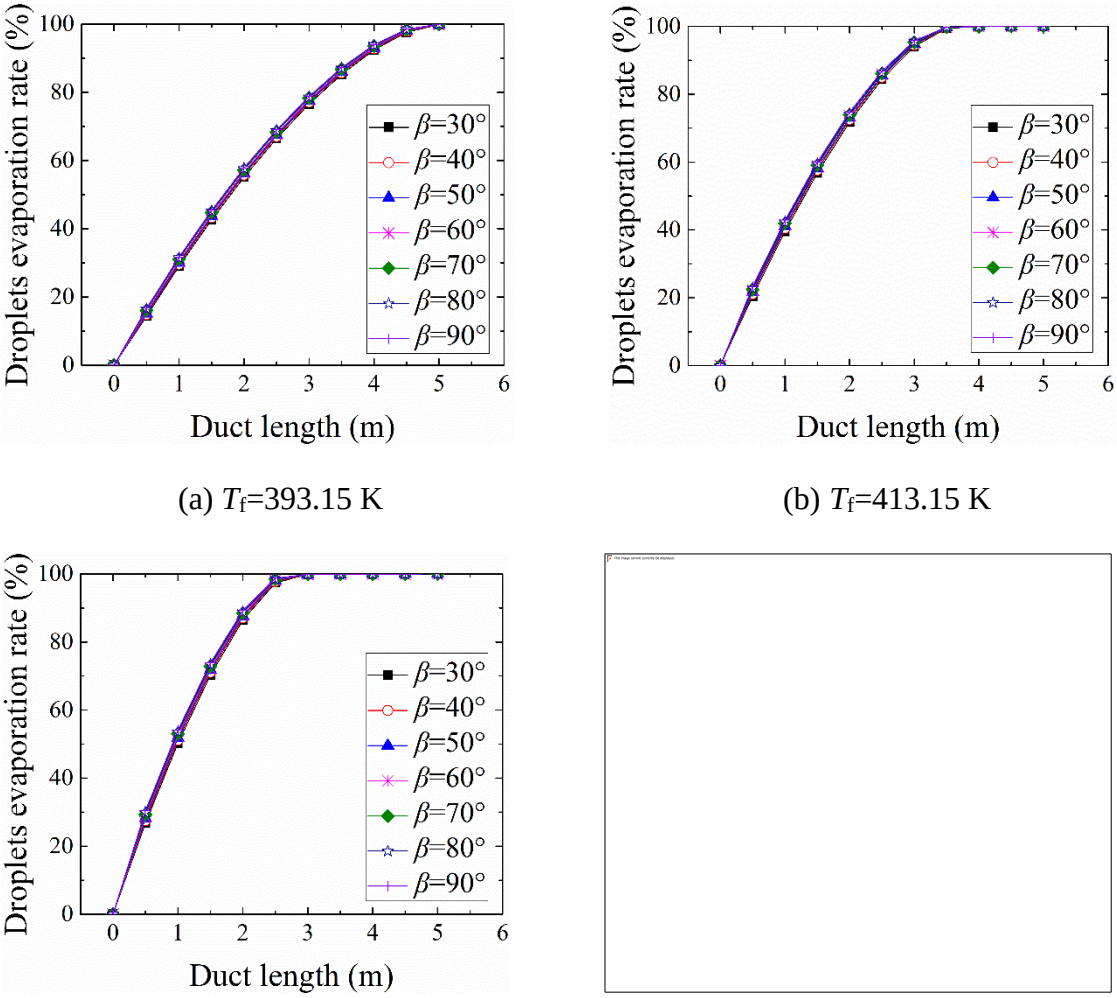

(a) T_f=393.15 K (b) T_f=413.15 K

(c) T_f=433.15 K (d) T_f=453.15 K

Fig. 14. The evaporation rate of atomized droplets at different nozzle spray full cone angles.

It can be seen from Fig. 14 that the droplet evaporation rate keeps an upward tendency with the increase of nozzle spray full cone angle, but the change is not obvious. Theoretically, the increase of nozzle spray full cone angle facilitates the formation of a larger conical spray cone so that the atomized droplet can fully diffuse in flue gas and thoroughly contact and exchange heat with flue gas, which contributes to shorter complete evaporation time and better droplets evaporation.

Nevertheless, the present flue gas flow rates have been provided sufficient heat source for atomized droplets evaporation with the given flue gas velocity and nozzle spray flow rate in the

studied conditions. Therefore, the improvement on droplet diffusion and evaporation is small with the increase of nozzle spray full cone angle. Thus, considering that atomized droplets might collide with the flue duct resulting in scale and corrosion on flue walls, the installation of nozzles with selected spray full cone angle only need to ensure that this phenomenon will not happen in practical engineering applications.

4.2.6 Spray direction of nozzle

The spray direction of nozzle plays an important role in droplets evaporation. The reference case has already been introduced in Table 3 as Case 6. The evaporation effects of atomized droplets sprayed in different directions under different inlet flue gas temperature conditions are demonstrated in Fig. 15.

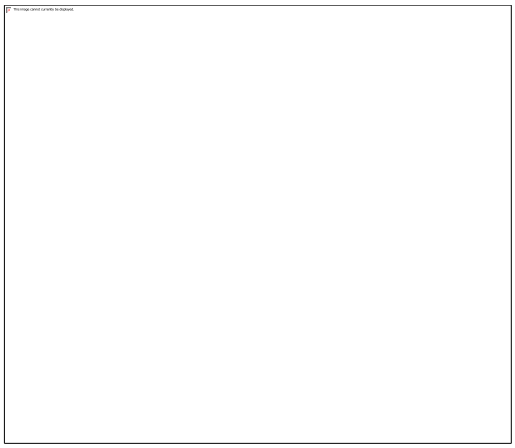

(a) T_f=393.15 K

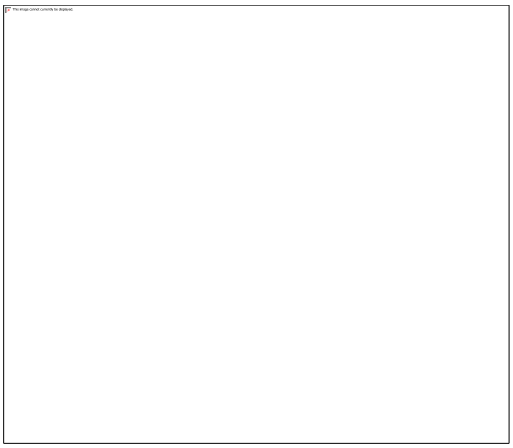

(b) T_f=413.15 K

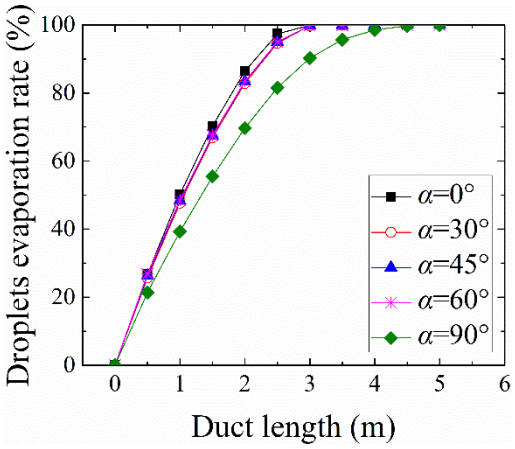

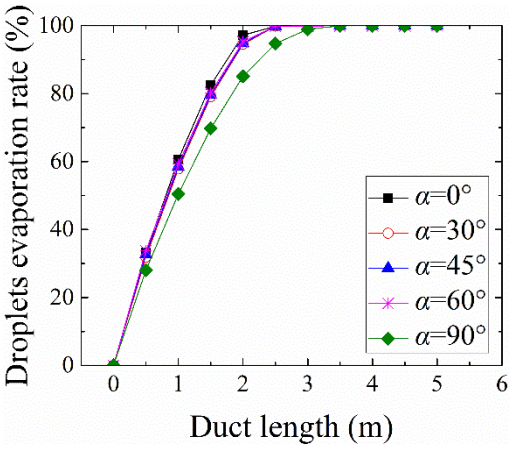

(c) T_f=433.15 K (d) T_f=453.15 K

Fig. 15. The evaporation rate of atomized droplets at different nozzle spray directions.

It can be seen from Fig. 15 that the evaporation rate of atomized droplets is the highest when the droplet spray direction is parallel to the flue gas flow direction. And the larger the angle between nozzle spray direction and flue gas flow direction is, the worse the droplets evaporation effect is.

Theoretically, the droplet residence time in flue gas will increase and the relative movement between flue gas and droplets will be enhanced with the adding angle between nozzle spray direction and flue gas flow direction. Thus, the promoted droplet dispersion and the reinforced heat transfer between flue gas and droplets can result in a wider range of heat exchange and more efficient droplets evaporation.

However, the nozzle spray direction has a great influence on the spatial distribution of atomized droplets. Droplets sprayed in an increasing angle between nozzle spray direction and flue gas flow direction cannot completely diffuse in flue gas within a 5 m evaporation distance, making them cannot entirely contact and exchange heat with flue gas and resulting in poor evaporation quality.

Taking the condition with 393.15 K inlet flue gas temperature as an example, the temperature field clouds of flue gas at different sections with different nozzle spray directions are shown in Fig. 16. These figures suggest that atomized droplets sprayed in an adding angle between nozzle spray direction and flue gas flow direction spread poorly in flue gas. Due to the adverse contact and heat transfer rate between droplets and flue gas, the evaporation effects are weakened with an increasing droplet spraying angle.

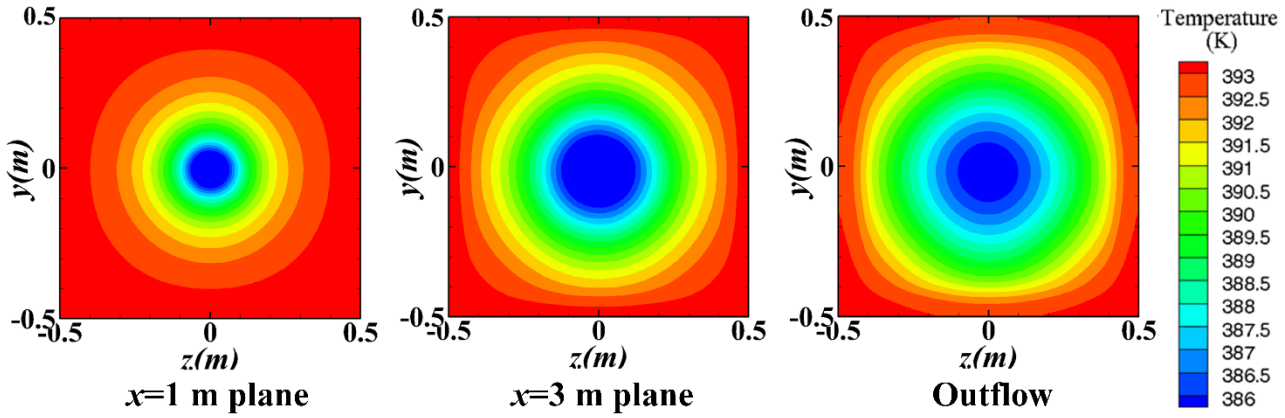

(a) α=0 °

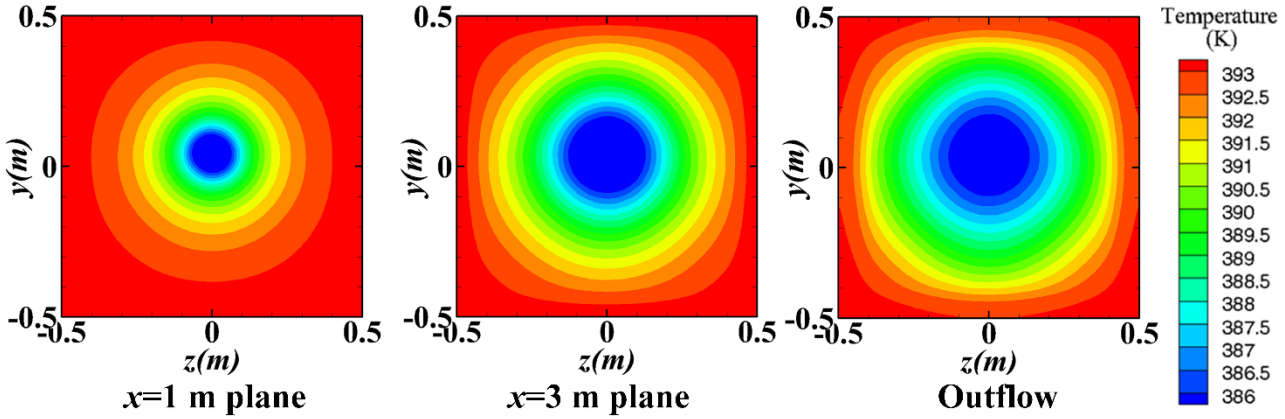

(b) α=30 °

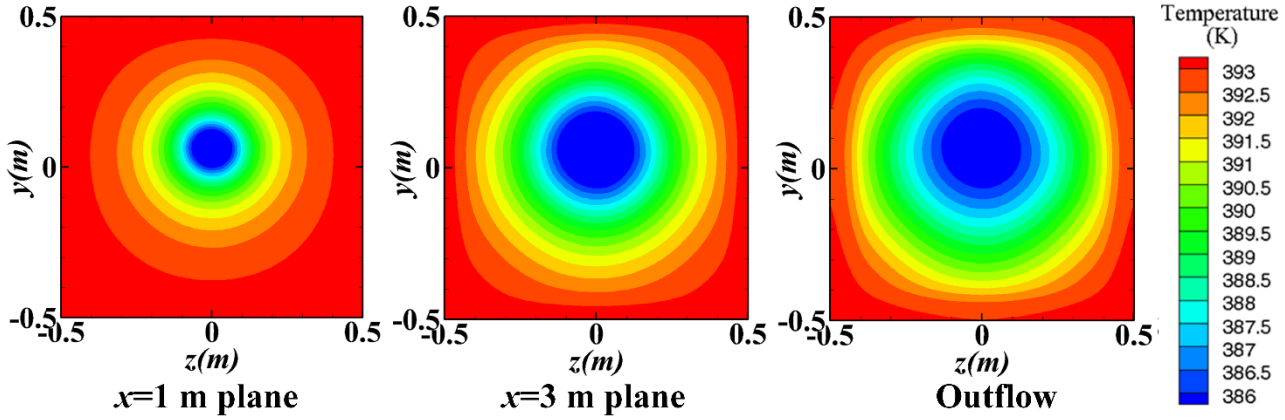

(c) α=45 °

(d) α=60 °

(e) α=90 °

Fig. 16. The temperature fields of flue gas at different cross sections in different nozzle spray directions.

Based on the above analysis, the spray direction of nozzle should be selected according to the specified length and shape of flue duct in practical engineering. More importantly, the enhanced relative movement between flue gas and atomized droplets as well as the droplets complete diffusion and full contact with flue gas for heat exchange must be taken into account at the same time, which are both the two crucial factors to heighten the droplets evaporation.

4.3 The LSSVM prediction on wastewater droplets evaporation in flue duct

To provide the basis for the process design and performance regulation of spraying FGD

wastewater in flue duct evaporation treatment under the comprehensive consideration of all above-mentioned factors, a multi-input-single-output least squares support vector machine (LSSVM) prediction model on droplet evaporation is established. The model can be employed to predict the droplet evaporation rate at different distances under various operating conditions.

In order to validate the feasibility and validity of the model, a total of 1600 sets of numerical data based on all the above simulations are taken as the sample data to build the LSSVM prediction model. Among them, 1200 sets of numerical data are taken as training data while 400 sets are used as test data. Eight variables, namely the initial diameter and velocity of atomized droplets, the temperature and velocity of flue gas, the spray flow rate, spray full cone angle and spray direction of nozzle and different evaporation distances, are selected as input variables. The droplet evaporation rate at different distances under different conditions is used as an output variable.

Firstly, 1200 sets of training data are used to train rolling for the learning capacity of LSSVM prediction model on droplet evaporation, balancing the training accuracy and generalization performance of the model. After rolling optimization, the related parameters of the model can be obtained by cross validation. The optimization parameters are set to =10000 and =0.01 respectively, minimizing the root mean square error. And then, eight input variables mentioned above are set respectively the same as the simulation conditions and process parameters of 400 sets of test data, calculating output prediction on droplet evaporation rate at different distances.

The results are illustrated in Fig. 17. Fig. 17 (a) shows the fitting degree between practical value and estimated value of LSSVM model. It can be seen that the prediction results of the LSSVM prediction model have a good fit between the practical value and predicted value. Fig. 17 (b) shows the average relative error between practical value and estimated value of LSSVM model. Among them, the maximum relative error does not exceed 9% while the average relative error (ARE) is 2.16% and the root mean square error (RMSE) is 1.64%. It can demonstrate that the present LSSVM prediction model can be used to accurately forecast the droplet evaporation rate at different

distances under different conditions among the above simulation range.

Due to the high prediction accuracy and good interpolation performance of the present LSSVM model, the value of input variables can be set the same as the known process parameters under practical operating conditions in power plant to predict the droplet evaporation rate along the flue duct of boiler. The present predicting model can be used both for the optimization of nozzle selection and layout, as well as the technical control of FGD wastewater spray evaporation treatment in thermal power plants, ensuring the safe and efficient operation.

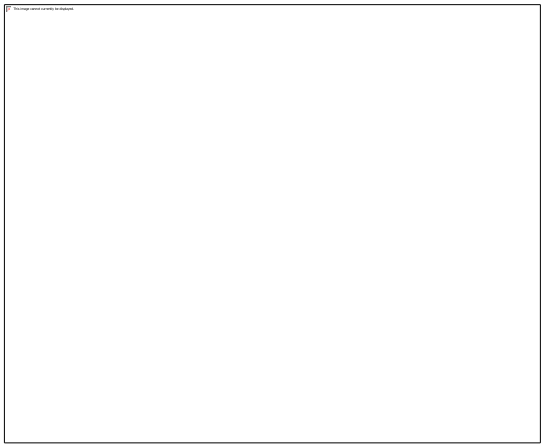

(a) Fitting degree between practical value and prediction of LSSVM model

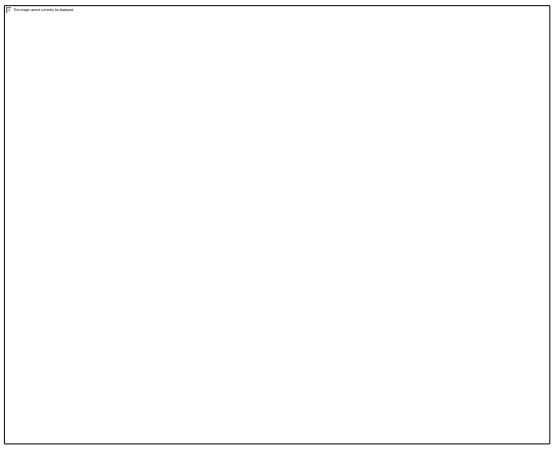

(b) Average relative error between practical value and prediction of LSSVM model

Fig. 17. Accuracy of the LSSVM predicting model.

5. Conclusions

The characteristics of droplets, flue gas and nozzle are the key heat transfer elements affecting the spraying FGD wastewater evaporation in the flue duct. Based on the combined Eulerian-Lagrangian mathematical model for the thermo-fluid behavior of FGD wastewater sprayed evaporation in the continuous flue gas, a study on the influencing factors under different operating conditions has been carried out by numerical simulation. And the LSSVM model is employed for forecasting the droplet evaporation rate while considering all the factors. The following conclusions can be obtained.

(1) The flue gas temperature and atomized droplets diameter have the dominating influences on the full evaporation distance of FGD wastewater in the flue duct, while the initial droplet velocity, flue gas velocity and spray full cone angle of nozzle all have little influences. The arrangement of multiple nozzles having small flow rate is proposed to improve the evaporation of atomized droplets.

(2) The spray direction of nozzles should be selected to ensure that the relative movement between atomized droplets and flue gas is enhanced, while the droplets with a good dispersion ability can contact and exchange heat with the flue gas within a specified distance and time, achieving the maximum evaporation of atomized droplets.

(3) The LSSVM prediction model on droplets evaporation has a high accuracy and can be carried out for the optimization of FGD wastewater droplets spray treatment technology under practical operating conditions in power plant.

Acknowledgements

The financial supports from the National Natural Science Foundation of China (No. 51676069), the National Key R&D Program of China (No. 2018YFB0604303) and the Royal Academy of Engineering (DVF1718\8\26) are gratefully acknowledged.

References

[1] J. J. Deng, L. M. Pan, D. Q. Chen, Y. Q. Dong, C. M. Wang, H. Liu, M. Q. Kang, Numerical simulation and field test study of desulfurization wastewater evaporation treatment through flue gas, Water Sci. Technol. 70 (2014) 1285-1291.

[2] B. Guan, W. Ni, Z. Wu, Y. Lai, Removal of Mn (II) and Zn (II) ions from flue gas desulfurization wastewater with water-soluble chitosan, Sep. Purif. Technol. 65 (2009) 269-274.

[3] Y. H. Huang, P. K. Peddi, C. Tang, H. Zeng, X. Teng, Hybrid zero-valent iron process for removing heavy metals and nitrate from flue-gas-desulfurization wastewater, Sep. Purif. Technol. 118 (2013) 690-698.

[4] Y. H. Huang, P. K. Peddi, H. Zeng, C. L. Tang, X. Teng, Pilot-scale demonstration of the hybrid zero-valent iron process for treating flue-gas-desulfurization wastewater: part I, Water Sci. Technol. 67 (2013) 16-23.

[5] Y. H. Huang, P. K. Peddi, H. Zeng, C. L. Tang, X. Teng, Pilot-scale demonstration of the hybrid zero-valent iron process for treating flue-gas-desulfurization wastewater: part II, Water Sci. Technol. 67 (2013) 239-246.

[6] H. Huang, J. Yang, D. Li, Recovery and removal of ammonia–nitrogen and phosphate from swine wastewater by internal recycling of struvite chlorination product, Bioresour. Technol. 172 (2014) 253-259.

[7] W. A. Shaw, Evaporation of wastewaters from wet gas scrubbing operations, International Pittsburgh Coal Conference, Pittsburgh, USA, 2008.

[8] A. Collin, P. Boulet, G. Parent, D. Lacroix, Numerical simulation of a water spray-Radiation attenuation related to spray dynamics, Int. J. Therm. Sci. 46 (2007) 856-868.

[9] H. Montazeri, B. Blocken, J. L. M. Hensen, CFD analysis of the impact of physical parameters on evaporative cooling by a mist spray system, Appl. Therm. Eng. 75 (2015) 608-622.

[10] J. Tissot, P. Boulet, F. Trinquet, L. Fournaison, H. Macchi-Tejeda, Air cooling by evaporating droplets in the upward flow of a condenser, Int. J. Therm. Sci. 50 (2011) 2122-2131.

[11] A. Alkhedhair, H. Gurgenci, I. Jahn, Z. Q. Guan, S. Y. He, Numerical simulation of water spray for pre-cooling of inlet air in natural draft dry cooling towers, Appl. Therm. Eng. 61 (2013) 416-424.

[12] A. Alkhedhair, I. Jahn, H. Gurgenci, Z. Q. Guan, S. Y. He, Y. S. Lu, Numerical simulation of water spray in natural draft dry cooling towers with a new nozzle representation approach, Appl. Therm. Eng. 98 (2016) 924-935.

[13] G. Lorenzini, O. Saro, Thermal fluid dynamic modelling of a water droplet evaporating in air, Int. J. Heat Mass Transfer 62 (2013) 323-335.

[14] J. D. Sartor, C. E. Abbott, Prediction and measurement of the accelerated motion of water drops in air, Appl. Meteor. 14 (1975) 232-239.

[15] J. Tissot, P. Boulet, A. Labergue, G. Castanet, F. Trinquet, L. Fournaison, Experimental study on air cooling by spray in the upward flow of a heat exchanger, Int. J. Therm. Sci. 60 (2012) 23-31.

[16] R. Sureshkumar, S. R. Kale, P. L. Dhar, Heat and mass transfer processes between a water spray and ambient air - I. Experimental data, Appl. Therm. Eng. 28 (2008) 349-360.

[17] S. S. Kachhwaha, P. L. Dhar, S. R. Kale, Experimental studies and numerical simulation of evaporative cooling of air with a water spray - I. Horizontal parallel flow, Int. J. Heat Mass Transfer 41 (1998) 447-464.

[18] H. Kim, N. Sung, The effect of ambient pressure on the evaporation of a single droplet and a spray, Combust. Flame 135 (2003) 261-270.

[19] N. Ashgriz, A. L. Yarin, Handbook of atomization and sprays, New York: Springer-Verlag New York inc. (2011) 869-879.

[20] J. A. K. Suykens, J. Vandewalle, Least Squares Support Vector Machine Classifiers, Neural Process. Lett. 9 (1999) 293-300.

[21] H. Z. Liu, S. L. Wang, J. Y. Liu, LS-SVM Prediction Model Based on Phase Space Reconstruction for Dam Deformation, Adv. Mater. Res. 663 (2013) 55-59.

[22] A. Asfaram, M. Ghaedi, M. H. A. Azqhandi, A. Goudarzi, M. Dastkhoon, Statistical experimental design, least square-support vector machine (LS-SVM) and artificial neural network (ANN) methods for modeling of facilitated adsorption of methylene blue dye, RSC Advances 6 (2016) 40502-40516.

[23] J. X. Liu, Z. H. Jia, Telecommunication Traffic Prediction Based on Improved LSSVM, Int. J. of Pattern Recogn. Artif. Intell. 32 (2017) 1850007.

[24] X. Li, I. Zbiciński, A sensitivity study on CFD modeling of concurrent spray-drying process, Dry. Technol. 23 (2005) 1681-1691.

[25] H. Montazeri, B. Blocken, J. L. M. Hensen, Evaporative cooling by water spray systems: CFD simulation, experimental validation and sensitivity analysis, Build. Environ. 83 (2015) 129-141.

[26] N. A. Fuchs, Evaporation and droplet growth in gaseous media, J. Appl. Mech. 27 (1960) 55.

[27] R. B. Bird, W. E. Stewart, E. N. Lightfoot, Transport phenomena, J. JW. A. 28(1960):338–359.

[28] S. S. Sazhin, Advanced models of fuel droplet heating and evaporation, Prog. Energy Combust. Sci. 32 (2006) 162-214.

[29] W. E. Ranz, W. R. Marshall, Evaporation from drops: I, Chem. Engng. Prog. 48 (1952) 141-146.

[30] W. E. Ranz, W. R. Marshall, Evaporation from drops: II, Chem. Engng. Prog. 48 (1952) 173-180.

[31] T. C. Jen, L. Li, W. Cui, Numerical investigations on cold gas dynamic spray process with nano- and microsize particles, Int. J. Heat Mass Transfer, 48 (2005) 4384-4396.

[32] Y. Hou, Y. Tao, X. Huai, Numerical characterization of multi-nozzle spray cooling, Appl. Therm. Eng. 39 (2012) 163-170.

[33] D. T. Chong, Numerical Investigation of Two-Phase Flow in Natural Gas Ejector, Heat Transfer Eng. 35 (2014) 738-745.

[34] A. B. Liu, D. Mather, R. D. Reitz, Modeling the effects of drop drag and breakup on fuel sprays, SAE Paper. (1993) 930072.

[35] P. Rosin, E. Rammler, The laws governing the fineness of powdered coal, J. Inst Fuel. 31 (1933) 29-36.

[36] H. Montazeri, B. Blocken, J. L. M. Evaporative cooling by water spray systems: CFD simulation, experimental validation, and sensitivity analysis, Build. Environ. 83 (2015) 129-141.

[37] P. J. O'Rourke. Collective Drop Effects on Vaporizing Liquid Sprays, PhD thesis. Princeton University. (1981).

[38] P. J. O'Rourke, A. A. Amsden. The TAB Method for Numerical Calculation of Spray Droplet Breakup, SAE Technical Paper 872089 (1987).

[39] S. M. Yang, W.Q. Tao, Heat Transfer, 4th edition, Higher Education Press. (2006) 560. (in Chinese)

Table captions

Figure captions

Fig. 15. The evaporation rate of atomized droplets at different nozzle spray directions. (a) T_f=393.15 K. (b) T_f=413.15 K. (c) T_f=433.15 K. (d) T_f=453.15 K.

Fig. 16. The temperature fields of flue gas at different cross sections in different nozzle spray directions. (a) α=0 °. (b) α=30 °. (c) α=45 °. (d) α=60 °. (e) α=90 °.

Fig. 17. Accuracy of the LSSVM predicting model. (a) Fitting degree between practical value and prediction of LSSVM model. (b) Average relative error between practical value and prediction of LSSVM model.